Applied Surface Science 613 (2023) 156026

Contents lists available at ScienceDirect

Applied Surface Science

journal homepage: www.elsevier.com/locate/apsusc

Full length article

Selective and reversible surface complexation of aqueous palladium(II) by polycarboxylate (pyromellitic acid) functionalized hybrid aerogel sorbent

Petra Herman [a], Krisztián Moldován [a,b], Geo Paul [c], Leonardo Marchese [c], Zoltán Balogh [a,b,d], Adél Len [d], Zoltán Dudás [d], István Fábián [a], József Kalmár [a,*]

[a] ELKH-DE Mechanisms of Complex Homogeneous and Heterogeneous Chemical Reactions Research Group, Department of Inorganic and Analytical Chemistry, University of Debrecen, Egyetem tér 1, Debrecen H-4032, Hungary
[b] Doctoral School of Chemistry, University of Debrecen, Egyetem tér 1, Debrecen H-4032, Hungary
[c] Department of Science and Technological Innovation, Università del Piemonte Orientale, Viale T. Michel 11, 15121 Alessandria, Italy
[d] Neutron Spectroscopy Department, Centre for Energy Research, Konkoly-Thege Miklós út 29-33, Budapest H-1121, Hungary

ARTICLE INFO

Keywords:
Aerogel
Palladium
Selective sorption
Surface complexation
Recovery

ABSTRACT

The recovery of palladium compounds from aqueous solutions containing other metal salts is a challenging task of environmental technology. One solution is the development of selective sorbents by the appropriate design of surface functionality. For this purpose, a mesoporous, polycarboxylate (pyromellitic acid monoamide) functionalized silica-gelatin aerogel was prepared by the sol-gel method and supercritical drying. It is characterized using low voltage scanning electron microscopy (LV-SEM), N_2-sorption porosimetry, small angle neutron scattering (SANS), infrared spectroscopy (FT-IR), solid-state nuclear magnetic resonance spectroscopy (ssNMR) and X-ray photoelectron spectroscopy (XPS). Its aqueous phase Zeta potential was investigated as a function of pH. The aerogel has excellent selectivity for binding Pd(II) around pH = 2.0 in the simultaneous presence of Pt(II), Pt (IV) and six other metal ions with a very high sorption capacity of 369 mg g^{-1} at pH = 2.3. The quantitative recovery of Pd(II) and the regeneration of the sorbent is possible using 5 mM methionine. The mechanism of binding is the reversible surface complexation of Pd(II) via the O-atoms of the adjacent carboxylate groups of the aerogel, as shown by XPS. This high stability coordination mode accounts for the excellent selectivity of the sorbent, and prevents the reduction of Pd(II).

1. Introduction

Palladium and its compounds have high technological importance and extensive use in petroleum refining, catalysis, electronics, pharmaceutics and many other fields. Elementary palladium dispersed in porous solid supports (e.g. in carbon) is an indispensable industrial catalyst [1]. Important organic coupling reactions (Sonogashira, Heck, Negishi, Suzuki) are based on palladium catalysts [2,3]. The oxidation- and corrosion resistant properties of this valuable metal enable a number of other technological applications (surge-resistor networks, jewelry, turbine blades for jet engines) [4,5]. The demand for Pd is especially high in the automobile and electronics industries as emission control catalysts and printed circuits [6,7]. Considering the technical, environmental and economic perspectives, the use of Pd and its compounds have limitations [8,9]. These are the high cost, low natural abundance, toxicity and environmental hazard. The recovery of platinum-group metals from secondary resources is a key challenge for achieving circular economy [5,10,11].

Palladium and its compounds are present as minor active components in industrial formulations. Accordingly, the spent catalysts, disposed electrical equipment, industrial and nuclear wastes contain high amounts of other metals (e.g., Fe, Cu, Zn, Ca, Mg) and their compounds [11,12]. Platinum usually accompany palladium and have similar chemical properties. The chief challenge of recovering palladium is the separation of these diverse components. Various methods have been reported for the recovery of palladium and its compounds, and most of them aim for the immobilization of aqueous Pd(II) as the final step using liquid-liquid or solid phase extraction, membrane separation, ion exchange, precipitation, sorption or reverse osmosis [13–15]. Sorption stands out from these methods, because of its cost effectiveness, ease of operation and high performance even at low Pd(II) concentrations [16]. The recovery of elementary palladium involves the

* Corresponding author.
E-mail address: kalmar.jozsef@science.unideb.hu (J. Kalmár).

https://doi.org/10.1016/j.apsusc.2022.156026
Received 16 September 2022; Received in revised form 20 November 2022; Accepted 6 December 2022
Available online 10 December 2022
0169-4332/© 2022 The Author(s). Published by Elsevier B.V. This is an open access article under the CC BY-NC-ND license (http://creativecommons.org/licenses/by-nc-nd/4.0/).

dissolution of the metal in acids, because Pd(II) compounds are stable and easy to handle in acidic solutions. Thus, the selective binding of Pd (II) has to be realized in acidic media, where sorption is one of the few feasible options.

Biocompatible, natural or bio-waste derived, composite or hybrid materials with well-designed functionalization can yield cost-effective and environmentally friendly selective sorbents with high capacities. Due to their chelating functional groups and chemical stability, biopolymers (chitosan, gelatin, alginate) are frequently used eco-friendly platforms [17–21]. High sorption capacities were reported for binding metal ions with glutaraldehyde crosslinked chitosan and cyclodextrin grafted chitosan [22,23]. Introducing sulfur containing soft Lewis bases (mercaptobenzimidazole or mercaptobenzothiazole) for the complexation of the soft Pd(II) is a favorable route [24,25]. Porous oxides (e.g. silica, alumina) are excellent non-toxic supports [26–28]. Silica can be functionalized with amines, thiols, carboxylates for binding aqueous Pd (II) [29,30]. Polyethyleneimine (PEI) functionalized alumina shows high affinity towards Pd(II). Activated carbon, carbon nanotubes, graphene and graphene oxide hybridized with biopolymers are also frequently used platforms for advanced sorbents [31,32]. A chitosan-graphene oxide hybrid was reported to effectively bind Pd(II) [33,34]. Polymeric resins are promising platforms, as well [35–39]. High sorption capacities for binding Pd(II) were reported for Aliquat-336 ionic liquid impregnated biopolymers and for chitosan/graphene oxide composites; ca. 200 mg g^{-1} at initial Pd(II) concentrations of 1–150 mg L^{-1} (pH = 2.0–3.0) [28,33]. The sorption equilibrium was reached in 12 h, and the re-solubilization of Pd(II) was realized with thiourea. The effective recovery of palladium was realized from a spent industrial catalyst with a novel silica/graphene oxide nanocomposite sorbent both in batch and fixed bed designs. The selectivity of the sorbent was proved against several other metal ions, and its efficient regeneration was demonstrated [40]. Another successful approach for the selective sorption of Pd(II) from industrial wastewater was using ion-imprinted polymers (IIPs) grafted with polymer bushes to eliminate the interference of other ions in the water matrix [41].

A novel family of advanced sorbents are supercritically dried aerogels, such as silica, biopolymers, hybrids etc. [42–45] The open mesoporous structure and the high surface area together with appropriate functionalization result in high sorption capacity and selectivity. In the present study, we aimed to prepare functionalized hybrid aerogels for the high capacity and selective sorption of aqueous Pd(II). In order to maximize the selectivity towards Pd(II), the introduction of adjacent carboxyl groups in a single functional moiety was targeted. Adjacent polycarboxylate groups were not tested before for binding Pd(II) from complicated aqueous matrices. Therefore, biocompatible silica-gelatin hybrid gels were functionalized with adjacent carboxylate groups post-gelation in the sol-gel process, and finally dried using supercritical CO_2 to obtain mesoporous aerogels. The aerogel sorbent was designed by considering that the silica constituent provides high porosity, while the polycarboxylate moieties ensure high affinity towards Pd(II). The as-prepared aerogels were characterized by scanning electron microscopy (SEM), N_2 sorption porosimetry, infrared spectroscopy (IR), small angle neutron scattering (SANS) and solid state nuclear magnetic resonance spectroscopy (NMR). Batch sorption experiments were conducted using aqueous Pd(II), Pt(II), Pt(IV), Cd(II), Cu(II), Zn(II), Pb(II), Ca(II) and Mg (II). In order to explore the most important features of the aerogel sorbent, the effects of metal ion concentration, pH, temperature and contact time were systematically investigated. The coordination chemistry of the metal ions and the protonation states of the functional groups in the aerogels were considered for explaining the mechanism of sorption.

2. Experimental section

2.1. Materials and solutions

All of the fine chemicals ($(NH_4)_2CO_3$, $Pd(NO_3)_2 \cdot 2H_2O$, K_2PtCl_4, $PtCl_4$, K_2PtCl_6; $PtCl_2$; $Cu(NO_3)_2 \cdot 3H_2O$, $Cd(NO_3)_2 \cdot 4H_2O$, $Pb(NO_3)_2$, Zn $(CH_3COO)_2 \cdot 2H_2O$, $CaCl_2$, $Mg(CH_3COO)_2$, NaOH, $C_5H_{11}NO_2S$, $C_3H_7NO_2S$, H_3BO_3, (3-aminopropyl)trimethoxysilane (APTMS), pyromellitic dianhydride (PMDA), dimethylacetamide (DMAc), HNO_3, H_2O_2, HF, CH_3OH, acetone were purchased from Sigma-Aldrich in ACS reagent grade and used without further purification. All aqueous solutions were prepared with ultrafiltered water ($\rho = 18.2$ MΩ cm by Milli-Q from Millipore). Tetramethyl orthosilicate (TMOS) and dimethyl sulfoxide (DMSO) was purchased from Fluka. Household gelatin sheets (type A, 150 kDa, food grade certified) were obtained from Dr. Oetker ensuring the high and constantly guaranteed quality of the product. Supercritical CO_2 was produced from 99.5 + % pure gas (Linde). A Metrohm 888 Titrando automatic titrator unit equipped with a double-junction 6.0255.100 pH electrode with KNO_3 as outer electrolyte was used to measure the pH of the solutions. Because some metal ions may form Cl^- precipitates and complexes, common single junction electrodes containing KCl electrolyte were not be used in this study. The desired pH was set by adding appropriate amounts of HNO_3 solution to the samples.

2.2. Synthesis of aerogels

2.2.1. Silica-gelatin hybrid aerogel (SG)

Pristine silica-gelatin hybrid aerogel (SG) was prepared using a previously published method without modification [46]. Briefly, two solutions (A and B) were prepared. Solution A was made from 4.0 mL TMOS dissolved in 16.0 mL DMSO. Solution B was 1.0 g gelatin dissolved in 5.4 mL hot water and 16.0 mL DMSO. The two solutions were mixed under vigorous stirring, then poured into a plastic mold. After 24 h, the fresh gel was transferred into a perforated frame and the sample was soaked in a mixture of acetone and DMSO for another 24 h. The solvent was replaced in every 24 h using a new solvent of increasing acetone content. Finally, the sample was stored in pure acetone for 24 h, and the gel was dried using supercritical CO_2, as described in details previously [47]. The resulting pristine hybrid silica-gelatin aerogel (SG) contains 23 wt% gelatin.

2.2.2. Aminopropyl functionalized silica-gelatin hybrid aerogel (SG-NH_2)

In order to introduce aminopropyl functional groups to the silica moiety of the hybrid aerogel, a portion of the TMOS was replaced by APTMS. Again, two solutions (A and B) were prepared. Solution A was made from 3.0 mL TMOS and 1.0 mL APTMS dissolved in 16.0 mL DMSO. 1.0 g gelatin was dissolved in 5.4 mL hot water and 16.0 mL DMSO to give solution B. The two solutions were mixed under stirring to form the functionalized fresh gel. Solvent exchange and supercritical drying was performed using exactly the same protocol as described in the case of the parent SG aerogel. The resulting aminopropyl functionalized silica-gelatin hybrid aerogel is termed SG-NH_2.

2.2.3. Polycarboxylate functionalized silica-gelatin hybrid aerogel (SG-COOH)

Polycarboxylate groups were introduced to the silica moiety of the hybrid aerogel by reacting the wet SG-NH_2 gel with pyromellitic dianhydride (PMDA) [48]. The fresh SG-NH_2 gel was directly transferred from the DMSO-water solvent into a solution (100 mL) of 0.10 M PMDA dissolved in DMAc. After 24 h reaction time, the functionalized wet gel was transferred to fresh DMAc–acetone 3:1 (*V*/V) mixture for 24 h. The solvent exchange was continued using DMAc–acetone 1:1; 1:3 and finally pure acetone, each for 24 h. Drying was performed using exactly the same protocol as for the other aerogels yielding polycarboxylate (pyromellitic acid monoamide) functionalized silica-gelatin hybrid aerogel (SG-COOH). The synthesis steps and the chemical structures of the aerogels are displayed in Scheme 1.

2.3. Aerogel characterization

The as-prepared aerogels were characterized using the following

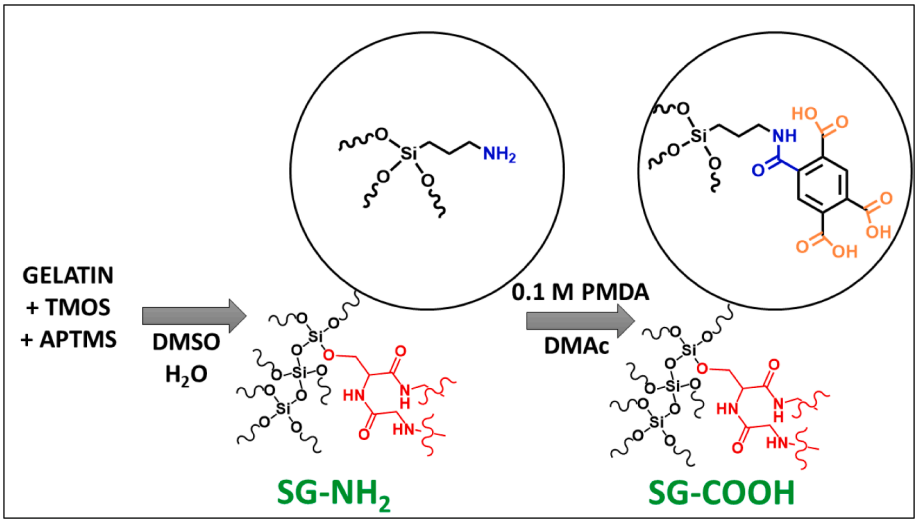

Scheme 1. Reaction scheme for the stepwise incorporation of aminopropyl, and subsequently polycarboxylate functional groups to the silica moiety of silica-gelatin hybrid gels.

experimental techniques: low voltage scanning electron microscopy (LV-SEM), N_2-sorption porosimetry, small angle neutron scattering (SANS), infrared spectroscopy (FT-IR), solid-state nuclear magnetic resonance spectroscopy (ssNMR) and X-ray photoelectron spectroscopy (XPS). The size distribution and the Zeta potential of the suspended aerogel particles were experimentally determined. Complete experimental details are given in the ***Supplementary Information*** for each technique.

2.4. Batch sorption experiments

The affinities of the suspended aerogels towards various aqueous metal ions were tested in batch sorption experiments at constant pH. A dilute HNO_3 solution of a pre-defined pH between 2.0 and 2.3 was used to prepare all suspensions, solutions and other aqueous mixtures. All solutions, suspensions and other mixtures were prepared and stored cc. HNO_3 treated glass vessels applicable for trace metal analysis.

Aqueous suspensions were prepared from the aerogels (c_{Agel} = 640 mg L^{-1}). The pristine aerogel was ground in a dilute HNO_3 solution using a Potter-Elvehjem tissue grinder for 10 min. This was followed by sonication (ARGO LAB DU-32) for 15 min and stirring for 20 min at 300 rpm using a magnetic stirrer and a 1.0 cm Teflon-coated rod. This procedure ensures the highly reproducible preparation of aerogel suspensions that do not settle or aggregate in the time scale of the sorption experiments.

Metal ion stock solutions were prepared in volumetric flasks by dissolving exact weights of solid metal salts in dilute HNO_3 solution. The pH of the stock solutions was adjusted to the desired value using the calibrated double-junction pH electrode. Metal ion solutions were prepared for the sorption experiments by the dilution of the stock solutions.

Batch sorption experiments were performed by mixing 4.00 mL metal ion solution of different concentrations and 4.00 mL aerogel suspension. The initial concentrations of the metal ions in the resulting 8.00 mL samples were between 10 and 200 mg L^{-1}. The heterogeneous samples were agitated with a magnetic stirrer typically for 2–4 h to reach sorption equilibrium. After the pre-set contact time, the samples were quantitatively transferred into plastic tubes (PP) and centrifuged for 20 min at 4700 rpm (VWR MEGASTAR 1.6 R). The supernatant was separated from the pellets, and the metal ion concentrations of the two phases were determined by elemental analysis using inductively coupled plasma optical emission spectrometry (ICP-OES). The initial concentrations of metal ions (c_0) were measured in control experiments. The final concentrations of the aqueous metal ions after the establishment of the sorption equilibrium were measured in the centrifugation supernatants. The concentrations of the metal ions were measured in the pellets, as well. All experiments were performed at least in three replicates. The applied analytical protocols are given in Section 2.9.

It was proved by independent experiments that the pH of a heterogeneous sample is constant during the batch sorption experiment. The maximum difference between the initial pH and the final pH in the separated supernatant was less than 0.16.

The above detailed experimental protocol was applied to investigate the sorption properties of the SG, SG-NH_2 and SG-COOH aerogels, as detailed in Sections 2.5, 2.7 and 2.8.

2.5. Selectivity of aerogel sorbent

The selectivity of the SG-COOH aerogel for Pd(II) sorption was tested in the simultaneous presence of aqueous Pd(II), Cd(II), Cu(II), Zn(II), Pb(II), Ca(II), Mg(II) ions at pH = 2.0 [10]. Besides, the selectivity was also tested using solutions of Pd(II) + Pt(IV) in the form of $PtCl_4$ and K_2PtCl_6, and Pd(II) + Pt(II) in the form of $PtCl_2$ and K_2PtCl_4 [49]. The Pt(IV) and the Pt(II) species are notorious for their inertness, thus, it was investigated how elevated temperatures (60 and 70 °C) promote their sorption on SG-COOH. The initial concentrations of the metal ions were varied between c_0 = 10 to 200 mg L^{-1} in the selectivity experiments.

2.6. Hydrolysis of palladium(II)

In order to ensure the reliability of the results of the sorption experiments, the possibility of the spontaneous hydrolysis and precipitation of the metal ions was investigated. Metal ion solutions (10–200 mg L^{-1}) were prepared in an identical way as for the sorption experiments, but in the absence of a sorbent, agitated, centrifuged and analyzed to detect the spontaneous formation of precipitates.

The results revealed that the hydrolysis of aqueous Pd(II) is significant above pH = 2.5 in the applied initial metal ion concentration range, as detailed later in Section 3.2.3. Thus, all sorption experiments were conducted at 0.010–0.005 M acid concentrations (pH = 2.0–2.3). The hydrolysis of aqueous Pd(II) is taken into account based on the thermodynamic laws of solution equilibria, and the aqueous species distribution of Pd(II) is given in Section 3.2.3.

2.7. Time-resolved experiments, kinetics of sorption

In order to study the rate at which the sorption equilibrium is

reached, time-resolved experiments were carried out at $c_0 = 80$ and 160 mg L^{-1} metal ion concentrations at pH = 2.0. The same protocol was used as in case of the batch experiments, but the length of the contact time was varied between 5 min and 24 h agitation.

2.8. Recovery of Pd(II), sorbent regeneration

The recovery of Pd(II) and the reversibility of its binding was tested by washing the previously equilibrated aerogels with either cysteine or methionine (5 mM; pH = 2.0) solutions. Essentially, the same experimental protocol was applied as in the sorption experiments. After centrifuging the equilibrium mixture of the aerogel and Pd(II) solution, the supernatant was quantitatively decanted and analysed for Pd(II). Subsequently, 8.00 mL of regenerating solution was added to the leftover aerogel pellet at pre-set pH. The aerogel was suspended, agitated for 1 h and centrifuged for a second time. The pellet and the supernatant were separated and analyzed. The regenerated aerogel was re-suspended in 8.00 mL dilute HNO_3 solution (pH = 2.0) to remove the traces of leftover cysteine or methionine. The system was centrifuged again and the supernatant was discharged. The regenerated aerogel was suspended in 4.00 mL dilute HNO_3 solution (pH = 2.0) and tested again for Pd(II) sorption. Altogether, three sorption-regeneration cycles were performed with one individual sample of aerogel.

2.9. Elemental analysis by ICP-OES

The experimental details for the ICP-OES analysis of the aerogel pellets and the various supernatants are given in the ***Supplementary Information***.

2.10. X-ray photoelectron spectroscopy (XPS)

X-ray photoelectron spectroscopy measurements were performed in order to determine the chemical structure of the aerogel sorbent, as well as, that of the bound palladium. The experimental details are given in the ***Supplementary Information***.

3. Results and discussion

3.1. Aerogel characterization

3.1.1. Scanning electron microscopy (SEM)

Representative SEM images of the as-prepared aerogels are shown in Fig. 1. The hybrid aerogel backbone is built from primary spherical nanoparticles that are covalently connected to each other forming an open porous network, which is characteristic for silica aerogels and silica-based hybrids [46,50]. The fundamental skeletal nanostructures of the SG, SG-NH_2 and SG-COOH aerogels are the same, independently of the functionalization; however the surface morphologies are distinct, as follows. The morphology of the pristine SG is similar to that of the archetypical silica aerogel. All the studied aerogels are mesoporous. Besides mesopores, a number of macropores are visible in the SEM images, especially in the case of the functionalized aerogels. The introduction of the aminopropyl (SG-NH_2), and subsequently the polycarboxylate functional groups (SG-COOH) results in the formation of a large number of macropores. Still, the total porosity of the different aerogels is approximately the same, as discussed in Sections 3.1.2 and 3.1.3. The incorporation of the polycarboxylate functional groups cause the visible coarsening of the aerogel backbone. This is indicative of the partial aggregation of the primary nanoparticles. These new superstructures in the backbone result in formation of wide ridges, and consequently, larger macropores.

3.1.2. N_2 adsorption-desorption porosimetry

Representative N_2 adsorption-desorption isotherms of the silica-gelatin aerogels are shown in Fig. 2A. All hysteresis curves are classified to be IUPAC IV category with a H3 type loop. This is characteristic for mesoporous materials with some macropores, which may not be completely filled with the N_2 condensate during measurement [51]. The position of the hysteresis loops is different for the functionalized SG-NH_2 and SG-COOH aerogels compared to the pristine SG, which is in accordance with the marked morphological changes observed in the SEM images. The adsorption-desorption curves reflect that the pristine SG is dominantly mesoporous, while many macropores are present in SG-NH_2 and SG-COOH. All desorption curves return to zero relative pressure, meaning that the rigidity of the aerogel backbones is intact during the N_2-sorption measurements.

The structural parameters calculated from the isotherms by the BET and the BJH methods are given in Table 1. The apparent surface area of the SG aerogel is 742 $m^2\ g^{-1}$, which is reasonable in comparison with previous results [46]. The apparent surface areas of the functionalized aerogels are smaller than that of the parent SG according to the N_2-sorption measurements, and it is the smallest in the case of SG-COOH (382 $m^2\ g^{-1}$). The BJH pore size distribution curves in Fig. 2B are in good agreement with the morphological features observed in the SEM images.

The SG is mainly mesoporous with a mean pore size of ca. $d_{pore} = 25$ nm. The pore size distributions are significantly wider towards the larger pores in the case of the functionalized aerogels due to the presence of macropores. The maxima of the wide pore size distributions of the functionalized aerogels are approximately at the same position as for the SG. Taking into account the contribution of the large macropores, the overall porosity of the functionalized aerogels are estimated to be comparable to that of the parent SG.

The smaller apparent surface areas of the functionalized aerogels are due to the transformation of some of the mesopores into macropores that are larger than 200 nm, thus, out of the quantification range of the N_2-sorption method. This is also concluded in previous reports discussing the connection between the mechanism of the formation of amino-functionalized silica gels in co-gelation and the structure of the final functionalized aerogels [52–55]. These reports are in agreement with each other and suggest that the trend in the decreasing surface area with the increasing amino group content is due to the increasing rate of gelation and the incomplete formation of the silica network in the presence of the basic precursor (e.g. APTMS) in the co-gelation. In the case of SG-COOH, the introduction of the acidic reagent after gelation

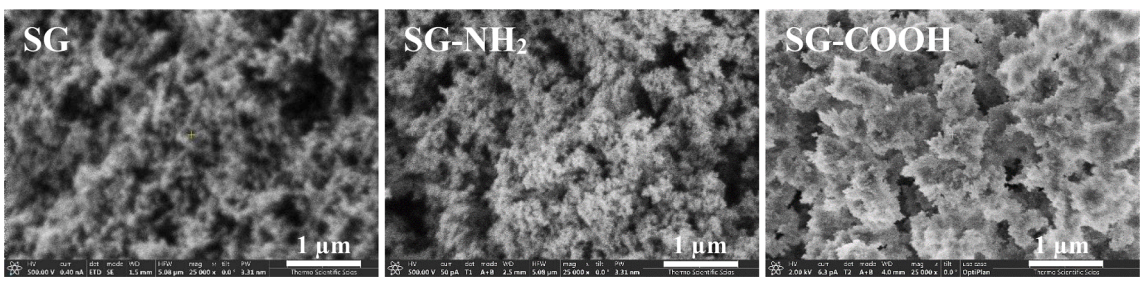

Fig. 1. LV-SEM images of the as-prepared silica-gelatin aerogels.

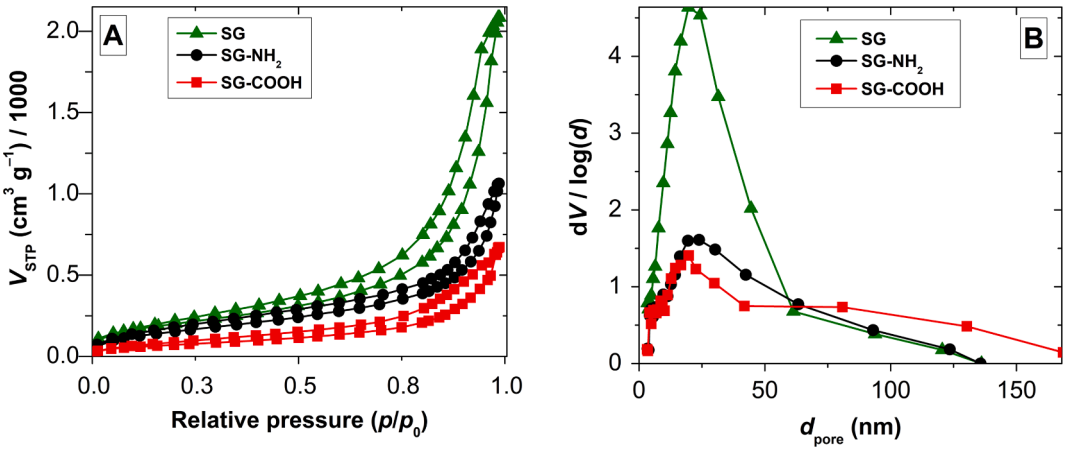

Fig. 2. Panel A: Nitrogen adsorption-desorption isotherms of the aerogels as given in the legend. Panel B: Pore size distribution curves calculated from the desorption isotherms using the BJH method.

Table 1
Structural parameters of the aerogels estimated by the BET and the BJH methods from N_2 adsorption-desorption porosimetry data in Fig. 2. Due to the limitations of the technique, the estimated parameters are valid for the pore size range from 3 to 170 nm.

	SG	SG-NH_2	SG-COOH	Data evaluation
C-constant	61 ± 2	39 ± 4	33 ± 3	BET
Specific surface area (m^2 g^{-1})	742 ± 35	589 ± 17	382 ± 20	BET
Average pore size (nm)	14 ± 2	24 ± 2	20 ± 2	BJH
Total pore volume (cm^3 g^{-1})	3.2 ± 0.1	1.5 ± 0.2	1.4 ± 0.1	BJH

induces minor secondary condensation reactions in the network, which alters the pore sizes for a second time.

3.1.3. *Small angle neutron scattering (SANS)*

The experimental scattering curves of the aerogels together with the results of the non-linear fitting are shown in Fig. 3. The Beaucage model (eq. S2 in the ***SI***) was used for data fitting in the middle and high Q ranges and the power-law model (eq. S3 in the ***SI***) in the low Q range. The estimated structural parameters are listed in Table 2. The R_g values of the Beaucage model represent the mean pore sizes of the aerogels (cf. eq. S4 in the ***SI***) [50,56]. The trend in the pore diameters from SG to SG-COOH is in good agreement with the measured widening of the pore size distributions towards the macropores as seen in Fig. 2B. Thus, the SANS, the N_2-sorption and the SEM data are in good agreement, and reflect the dramatic increase of the pore sizes as the consequence of the functionalization of the aerogels.

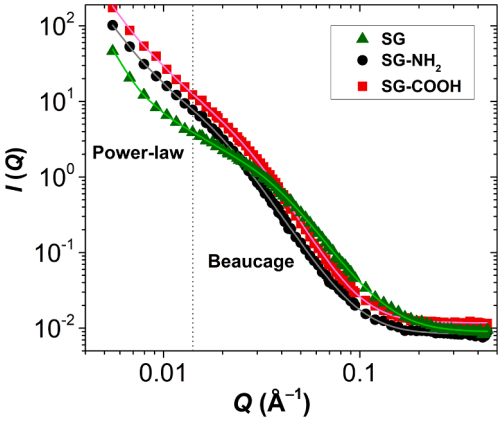

Fig. 3. Experimental small angle neutron scattering (SANS) curves of the aerogels (markers), and the results of non-linear fitting using Eqs. 2 and 3 (solid lines). The estimated parameters are given in Table 2.

Table 2
Structural parameters estimated by fitting the SANS curves of silica-gelatin aerogel samples with the Beaucage and power-law models. The experimental and the fitted SANS curves are shown in Fig. 3.

	Beaucage model [high Q region]			Power-law [low Q region]
	p_1	R_g (Å)	d_{pore} (nm)[a]	p_2
SG	3.51 ± 0.03	114 ± 2	29.9	5.0 ± 0.1
SG-NH_2	3.80 ± 0.02	228 ± 8	59.7	3.9 ± 0.1
SG-COOH	4.10 ± 0.02	169 ± 5	44.3	4.1 ± 0.1

[a] Calculated from the R_g values using eq. S4 in the ***SI***.

Additional morphological information can be deduced from the SANS data based on the p values estimated in the different Q ranges (Table 2) [57,58]. The p_1 value of the Beaucage model estimated in the high Q region reflects the fractal-like nanostructure of the surface of the aerogel backbone, which is built from primary nanoparticles [59]. The p_1 values of ca. 3.5 and 3.8 for the SG and the SG-NH_2 aerogels, in order, are characteristic for surface fractals, showing the roughness of the aerogel backbone bordering the pores. In contrast, the $p_1 \approx 4$ value of the SG-COOH reflects a quasi-smooth backbone-pore interface. This can be the consequence of the aggregation and merger of the primary nanoparticles, which in one hand smooths out the roughness of the surface of the pore walls, and on the other hand results in the formation of macropores visible in the SEM images (cf. Fig. 1). The p_2 value of the power-law model estimated in the lowest Q region is characteristic for the morphology of the aerogel in the sub-micrometers scale, comparable to SEM imaging [59]. In this scale, the microstructure of SG is quasi-homogeneous, but contains a density gradient, as reflected in the p_2 value of 5.0. The reason can be the uneven distribution of the primary nanoparticles on the scattering surface. The microstructures of the SG-NH_2 and the SG-COOH aerogels consist of several ridges and macropores, especially in the case of the SG-COOH, as seen in the SEM images. The $p_2 \approx 4$ values estimated in the lowest available Q-range reflect the presence of smooth surfaces in the micrometers scale, which is due to the smooth walls of the large macropores.

The compiled data from SEM, N_2-sorption and SANS give a complete picture on both the microscale and the nanoscale structures of the aerogels. Importantly, the polycarboxylate functionalized SG-COOH aerogel is highly porous with an accessible and interconnected open pore

network, which is highly advantageous for its application as a sorbent.

The pore network of the parent SG aerogel has previously been investigated using contrast variation SANS measurements [46]. Matching the contrast of the aerogel backbone results in scattering practically equivalent to the background. This indicates that there are no closed pores retaining air pockets in the aerogel network,

3.1.4. FT-IR spectroscopy

The representative FT-IR spectra of the aerogels are shown in Fig. 4. The IR spectrum of a pure silica aerogel is also shown as a reference. All four IR spectra display an intensive broad peak at ca. 1065 cm^{-1} corresponding to Si–O–Si asymmetric stretching vibration, which is characteristic for silica-based aerogels. The symmetric vibration of the Si–OH bond is detected at ca. 950 cm^{-1}. These IR bands are typical for amorphous silica skeletons.

The peaks in the range of 2800–3400 cm^{-1} are assigned to various N–H and O–H of the peptide component of the SG hybrid aerogels. The intensive peaks at ca. 1650 cm^{-1} are characteristic for the symmetric and the asymmetric vibrations of the carboxylate and amide groups of the peptide chains in the hybrids. A narrow band is present at 1718 cm^{-1} in the spectrum of SG-COOH, which is typical of the C=O stretching vibration in free carboxylic groups [48]. This band is absent in the other spectra and serves clear evidence for the incorporation of the polycarboxylate functional groups into SG-COOH. Another unique feature of the IR spectra is a minor peak at 705 cm^{-1} which relates to the N–H bending vibrations of free amino groups. As expected, this peak is found only in the spectrum of SG-NH_2.

3.1.5. Solid state NMR

The ^{29}Si CPMAS, ^{13}C CPMAS and ^{1}H MAS NMR spectra of the aerogels are shown in Fig. 5. The assignments of the ssNMR peaks to the different structural elements in the aerogels are also shown in Fig. 5. The stepwise changes in the ssNMR spectra are in line with the expected chemical modifications in the applied synthesis steps. The incorporation of the new functional groups is verified by the ssNMR data. No major side products are detectable.

The structure of the silica backbone of the aerogels is evaluated using the ^{29}Si CPMAS NMR spectra, which show peaks at around −110, −101 and −91 ppm for the SG aerogel. These peaks are due to Q^4, Q^3 and Q^2 silicon units, respectively [60]. The SG-NH_2 and SG-COOH aerogels exhibit additional peaks at −66 and −58 ppm due to T^3 and T^2 silicon sites, confirming the anchoring of the aminopropyl groups into the silica backbone [60].

Additional information on the aerogels is obtained by ^{13}C CPMAS and ^{1}H MAS NMR spectroscopy. The ^{13}C CPMAS NMR spectrum of the SG is in close resemblance to spectrum of gelatin (data not shown) confirming the incorporation and the structural integrity of gelatin into the aerogels. Additional ^{13}C peaks are clearly visible in the spectrum of the SG-NH_2 aerogels that are due to the aminopropyl carbons, corroborating the ^{29}Si CPMAS NMR data. Finally, the polycarboxylate functionalization in the SG-COOH aerogel is evident based on the presence of peaks due to aromatic carbons (in the range of 120–145 ppm) and carboxylate carbons (169 ppm). These assignments are further supported by the ^{1}H MAS NMR data.

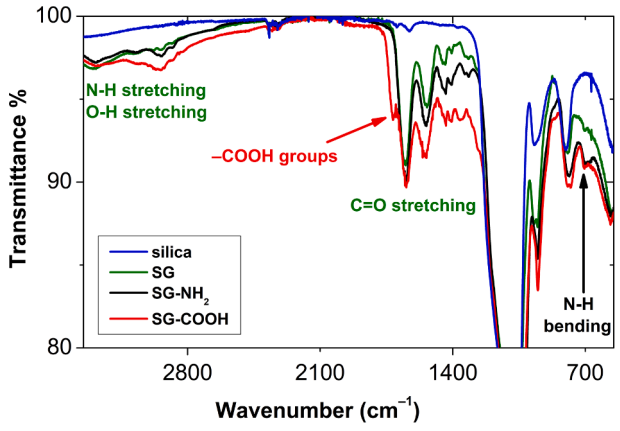

Fig. 4. Infrared spectra of the aerogels.

The overall conclusion drawn from the IR and the ssNMR data is that the chemical functionalization of the SG-NH_2 and SG-COOH aerogels are successful, and the structures of the functionalized aerogels satisfy the expectations (Scheme 1).

3.1.6. Size of hydrated aerogel particles

Silica-gelatin aerogels spontaneously disintegrate in water and yield characteristic micrometer-size particles as demonstrated in previous publications [61]. The particle size distributions of the suspended silica-gelatin aerogels were measured after wet grinding the samples. A narrow size distribution is observed for the SG aerogel. The mean size of the hydrated particles is ca. 6 μm. The functionalized aerogel particles have wider size distributions with hydrated particles in mean sizes ranging from 10 to 12 μm (Fig. 6).

3.1.7. Zeta potential of aerogel particles

The Zeta potentials of the suspended hybrid aerogel particles were measured in the pH range from 3.0 to 9.0 (Fig. 7). The SG and SG-NH_2 have approximately the same Zeta potentials of ca. +22 mV at pH = 3.0. The isoelectric points of SG and SG-NH_2 are at about pH = 3.8 and 4.1, respectively. The Zeta potentials of SG-NH_2 are significantly higher than those of the parent SG, regardless of pH, due to the presence of the primary amino groups. The opposite trend is observed for SG-COOH due to the presence of the polycarboxylate groups. The net charge of SG-COOH remains negative at pH = 3.0, but a steep increase in its Zeta potential is evident when the pH decreases to 3.0.

3.2. Sorption of aqueous Pd(II)

3.2.1. Sorption isotherms for SG, SG-NH_2 and SG-COOH aerogels

The physicochemical characteristics of the binding of Pd(II) to SG, SG-NH_2 and SG-COOH were investigated by measuring isotherms using different initial Pd(II) concentrations (c_0Pd(II) between 10 and 200 mg L^{-1}). Higher concentrations were not applied to avoid complications from the hydrolysis of Pd(II), as discussed later. Based on the experimental sorption isotherms shown in Fig. 8, all aerogels bind significant quantities of Pd(II), and SG-COOH has the highest sorption capacity.

In order to quantify the sorption equilibria, the experimental data were fitted with different isotherm models using non-linear regression algorithms. The adequacy of the different isotherm models was judged based on the goodness of the fit and the mechanistic background of the model. An important criterion is that the appropriate isotherm model should incorporate an upper limit for sorption at high metal ion concentrations defining the complete occupation of the active sites, and thus, the sorption capacity. The Freundlich model does not incorporate such a limit, therefore it cannot be used here for data fitting [62,63].

The simplest feasible model is the Langmuir isotherm, which assumes equivalent binding sites. However, the Langmuir model proved inadequate for fitting the experimental data in this case, because of the high curvature of the experimental isotherms. Instead, the Sips model (also termed as the Langmuir-Freundlich isotherm) performs well in describing the observed phenomena. The Sips model is based on the following considerations [62,63]. It is reasonable to assume that all of the studied aerogel sorbents contain different binding (coordination) sites for Pd(II), e.g. different functional groups, or the same functional group situated in different chemical environments. Thus, the coordination (binding) mode of Pd(II) is expected to show a high variation in different locations in the aerogel backbone, which can be approximated by formulating a distribution for the binding energy of Pd(II), as done by the Sips model [62,64,65]. Nevertheless, at high Pd(II) concentrations,

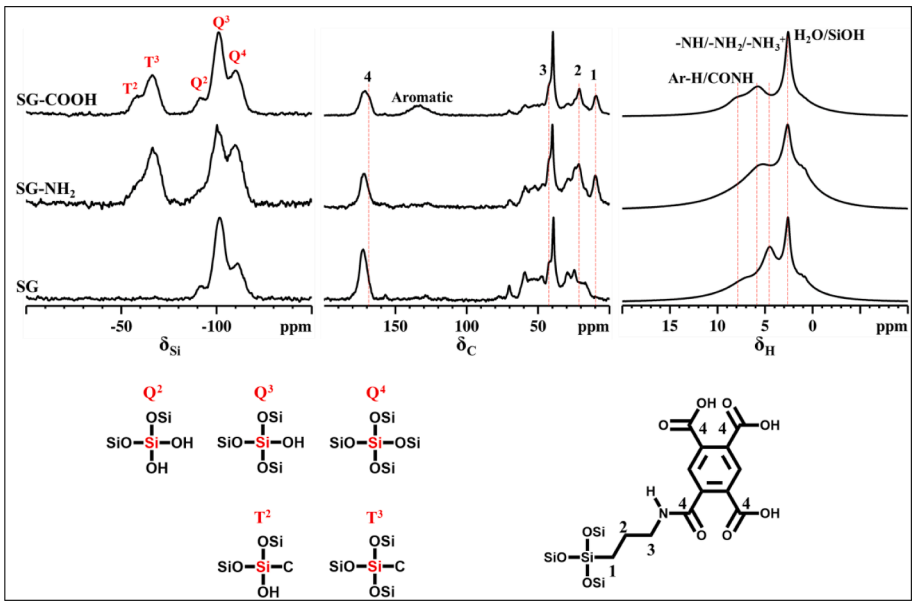

Fig. 5. Upper panel: Solid-state NMR (^{29}Si CPMAS, ^{13}C CPMAS, ^{1}H MAS) spectra of the aerogels. Lower panel: The assignments of the signals to the chemical structural elements.

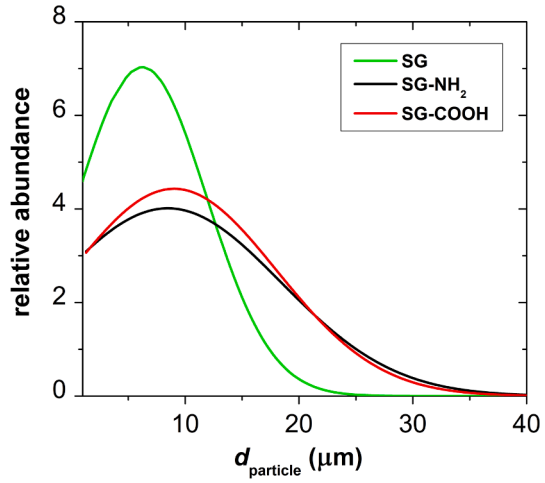

Fig. 6. Particle size distribution curves of hydrated aerogels measured by optical microscopy and image analysis.

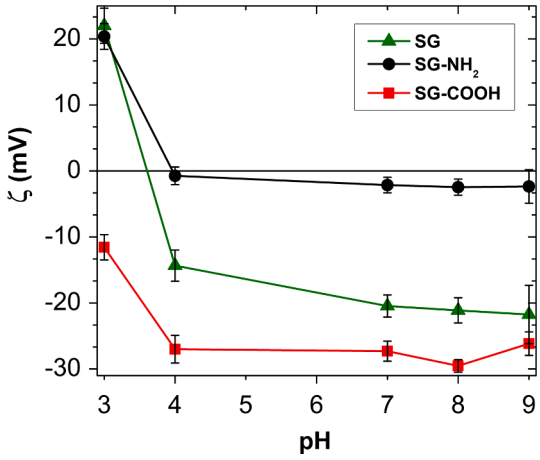

Fig. 7. The Zeta potentials of aqueous aerogel microparticles as a function of pH.

all active sites are expected to be saturated, which defines the maximum surface coverage in a quasi-monolayer on the sorbent. The Sips model does not specify the physicochemical nature of the binding of Pd(II), but assumes the existence of multiple dynamic equilibria in the different binding modes by extending the Langmuir model. Finally, the effect of the competitive reactions of Pd(II) in the aqueous phase (e.g. hydrolysis, complexation) can be neglected at constant pH, because the speciation of aqueous Pd(II) is independent of its final concentration in the solution.

In view of all these considerations, the Sips model is suitable for the formal description of Pd(II) sorption under the applied conditions at constant pH. (Naturally, the interactions affecting the binding of aqueous Pd(II) are regulated by the pH, which is discussed in details in Section 3.2.3.) The mathematical equation of the Sips isotherm is as follows:

$$q_E = \frac{[\mathrm{Pd(II)}]_{ads}}{c_{Agel}} = S\frac{(K_S[\mathrm{Pd(II)}]_{sol})^n}{1+(K_S[\mathrm{Pd(II)}]_{sol})^n} \quad (1)$$

Here, q_E is the amount of metal ions sorbed in equilibrium per unit mass of sorbent, (mg g^{-1}), $[\mathrm{Pd(II)}]_{ads}$ is the solution-equivalent concentration of sorbed Pd(II) in equilibrium (mg L^{-1}), c_{Agel} is the concentration of the aerogel (g L^{-1}) and $[\mathrm{Pd(II)}]_{sol}$ is the equilibrium concentration of aqueous Pd(II) (mg L^{-1}). S is the sorption capacity of the aerogel (mg g^{-1}), K_S is the Sips equilibrium constant (L mg^{-1}) and n is the dimensionless power constant.

The experimental isotherms were fitted using a non-linear least squares method based on the Levenberg-Marquardt algorithm. The fit is very good in each case. The fitted sorption isotherms are shown in Fig. 8 and the estimated parameters are given in Table 3. The estimated theoretical sorption capacities of the SG and SG-NH$_2$ aerogels are both ca. 150 mg g^{-1}. The incorporation of carboxyl groups significantly increased the sorption capacity of the SG-COOH aerogel to ca. 300 mg g^{-1} at pH = 2.0, with an equilibrium constant of $K_S = 0.019$ L^{-1} mg. The power constant is approximately uniform for the three aerogel sorbents: $n = 0.47$ (Table 3).

In practice, at relatively low initial concentrations of Pd(II) (c_0 = 10–30 mg L^{-1}) ca. 90–95% of Pd(II) is sorbed by SG-COOH using it at c_{Agel} = 0.32 g L^{-1}. The results obtained at higher initial Pd(II)

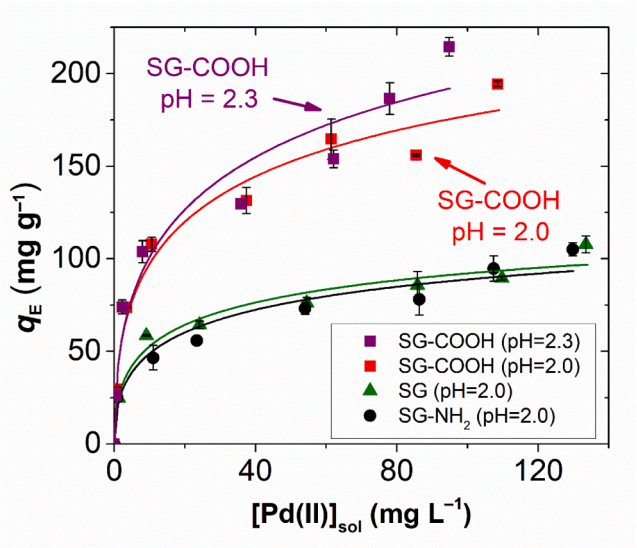

Fig. 8. Sorption isotherms of Pd(II) on SG, SG-NH_2 and SG-COOH hybrid aerogels at pH = 2.0 and 2.3. Symbols: experimental points. Lines: nonlinear least squares fits using the Sips isotherm model (eq. (1)). The estimated isotherm parameters are shown in Table 3. (c_{Agel} = 320 mg L^{-1}; c_0Pd(II) = 10–200 mg L^{-1}; T = 25 °C).

Table 3
Isotherm parameters estimated by fitting the experimental isotherms to the Sips model (eq. (1)). The fitted curves are displayed in Fig. 8.

	pH	S (mg g^{-1})	$K_S \times 10^2$ (L mg^{-1})	n
SG-COOH	2.3	369 ± 107	1.3 ± 0.9	0.47 ± 0.1
SG-COOH	2.0	307 ± 99	1.9 ± 1.0	0.46 ± 0.1
SG-NH_2	2.0	149 ± 21	2.8 ± 0.9	0.47 ± 0.1
SG	2.0	153 ± 24	2.0 ± 0.9	0.47 ± 0.1

concentrations show the sorption of more than 200 mg Pd(II) on 1.0 g aerogel. Owing to the high performance of SG-COOH, further experiments were performed to optimize the sorption process and the subsequent recovery of Pd(II).

Attempts were made to increase the sorption capacity of the SG-COOH aerogel by increasing the amount of the functional groups. This was realized in the synthesis by increasing the ratio of the –NH_2 bearing APTMS precursor, and subsequently, the corresponding amount of the acid anhydride. Unfortunately, the sorption capacity of SG-COOH could not be increase further, as demonstrated in the ***Supplementary Information***. The explanation is, that the increased amount of APTMS resulted in the decrease of the apparent surface area of the final aerogel, and consequently the altered the accessibility of the functional groups [52–55].

3.2.2. *Selectivity of SG-COOH aerogel*

The selectivity of SG-COOH towards aqueous Pd(II) was tested in the presence of multiple competing metal ions (cf. Section 2.5). First, the effect of Cd(II), Cu(II), Zn(II), Pb(II), Ca(II), Mg(II) were tested at pH = 2.0. The results confirm that SG-COOH has high selectivity for binding Pd(II), as seen in Fig. 9A.

Independent sorption measurements were carried out to test the selectivity of SG-COOH towards Pd(II) in the presence of different Pt(IV) and Pt(II) species, specifically aqueous $PtCl_2$, $[Pt^{II}Cl_4]^{2-}$, $PtCl_4$ and $[Pt^{IV}Cl_6]^{2-}$. The same species were tested as interfering ions in previous studies with other sorbents [10,18,19,21]. Interestingly, none of these platinum species showed significant affinity to bind to SG-COOH in the studied pH range. Only the $PtCl_2$, $[Pt^{II}Cl_4]^{2-}$ and $[Pt^{IV}Cl_6]^{2-}$showed minor binding. In order to test whether this is the consequence of the well-known inertness of the coordination of platinum ions, the sorption experiments were repeated at longer contact times (4–24 h) and higher temperatures (60–70 °C). As seen in Fig. 9B, the altered conditions did not significantly increase the amount of bound platinum species, therefore, did not compromise the selectivity of SG-COOH toward binding Pd(II), especially at lower temperatures.

This unprecedentedly high selectivity is a major advantage of the aerogel sorbent, because it allows the separation of Pd(II) even from the platinum ions that have very similar chemical properties. In several industrial applications, palladium compounds are accompanied by various other metal compounds, including platinum. The use of SG-COOH offers a versatile possibility for the selective recovery of Pd(II) from such acidic media.

3.2.3. *Effect of pH on the sorption of Pd(II)*

One of the most important factors controlling the kinetic and thermodynamic properties of sorption is the pH. It has a significant effect both on the hydrolysis of Pd(II), and on the protonation of the functional groups of the sorbent governing its surface charge.

The quantitative description of the hydrolysis of Pd(II) is important for understanding the mechanism of its binding to the aerogel and for determining the optimum pH for the sorption process. Fig. 10 shows the speciation of aqueous Pd(II) calculated using the published thermodynamic equilibrium constants [66,67]. The hydrolysis of Pd(II), i.e. the

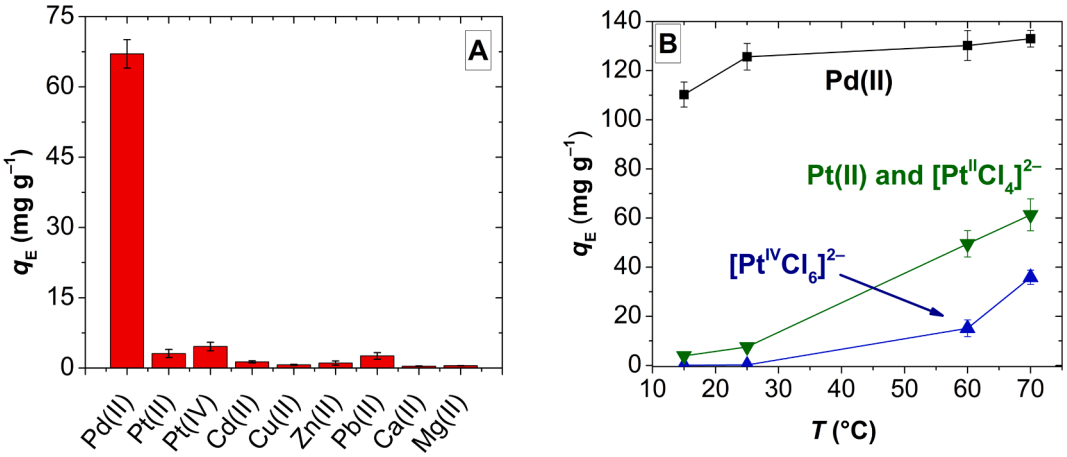

Fig. 9. Panel A: Amount of metal ions sorbed by the SG-COOH aerogel from a solution of multiple metal ions at pH = 2.0 (each metal ion: c_0Metal = 25 mg L^{-1}; c_{Agel} = 320 mg L^{-1}; T = 25 °C; 4 h agitation). Panel B: Sorption of Pd(II), Pt(II) and Pt(IV) as a function of temperature. The sorption of the Pt(II) and the Pt(IV) species were tested in the presence of Pd(II). (c_0Metal = 90 mg L^{-1}; c_{Agel} = 320 mg L^{-1}; 4 h agitation).

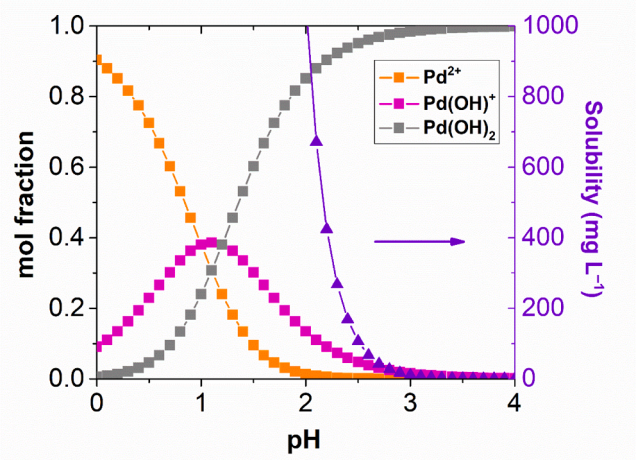

Fig. 10. The speciation and the solubility of aqueous Pd(II) as a function of pH.

formation of hydroxo-Pd(II) complexes, is significant even under highly acidic conditions and it is complete at ca. pH = 3.0 with the formation of the charge neutral $Pd(OH)_2$. Between pH = 1.0 and 2.0, Pd(II) exists mainly in the form of cations (Pd^{2+} and $PdOH^{+}$) in the absence of other ligands. In the applied pH range (pH = 2.0–2.3) the dominant species is $Pd(OH)_2$. Importantly, the solubility of $Pd(OH)_2$ (ca. 260 mg L^{-1} at pH = 2.3) is higher than the highest Pd(II) concentration used in the sorption experiments (c_0Pd(II) = 200 mg L^{-1}). In practice, the absence of hydroxide precipitate formation was confirmed in independent control experiments carefully designed to test the relevance of the hydrolysis of Pd(II) under the applied conditions (cf. Section 2.6).

The pH determines the protonation states of sorbent functional groups, as well. The Zeta potential of SG-COOH is negative at pH = 3.0 indicating negative surface charge, but steeply increases with decreasing pH (cf. Fig. 7). This implies that the carboxyl groups of the aerogel are at least partially protonated in the pH range of the sorption experiments (pH = 2.0–2.3). Deprotonated carboxylate groups in close proximity to each other are strong binding sites for Pd(II). Furthermore, the coordination of Pd(II) by adjacent carboxylate groups is favored even when the concerted loss of protons is required [68,69].

Overall, the decrease of pH has counterbalancing effects on the sorption process: it *i*) limits the hydrolysis of the metal ions, which is advantageous for their coordination to the surface functional groups, and it *ii*) partially protonates the carboxylate groups and increases the surface charge of the aerogel, which is disadvantageous for the binding of metal ions [70].

Considering that the solubility of aqueous Pd(II) is ca. 100 mg L^{-1} at pH = 2.5, and it is only ca. 10 mg L^{-1} at pH = 3.0, the formation of the hydroxo precipitate eventually interferes with the sorption process at higher pH, which could lead to the misinterpretation of the capacity of the sorbent. In order to avoid complications arising from the precipitation of Pd(II), the pH dependence of the sorption process was investigated at 0.010–0.005 M acid concentrations (pH = 2.0–2.3) in the present study.

The amount of sorbed Pd(II) in equilibrium (q_E), and the theoretical sorption capacity of SG-COOH is significantly higher at higher pH, as seen in Fig. 8 and Table 3. A practical aspect is optimizing the sorption process at highly acidic pH is relevant for possible industrial applications considering that the valuable metal compounds have to be recovered from various secondary resources using acidic reagents in selected technological steps [71].

3.2.4. Time-resolved experiments, kinetics of sorption

Time-resolved sorption experiments were performed using min. 5 min and max. 24 h agitation time. The sorption equilibrium is practically established in 2 h contact time, as seen in the kinetic curves in Fig. 11.

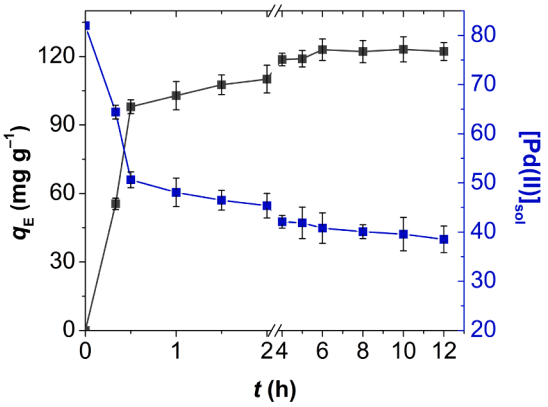

Fig. 11. Kinetics of sorption. The amount of bound Pd(II) in the SG-COOH hybrid aerogel (black markers) and the change of the aqueous Pd(II) concentration (blue markers) as a function of the contact time. (c_0Pd(II) = 80 mg L^{-1}; c_{Agel} = 320 mg L^{-1}; pH = 2.0; T = 25 °C). (For interpretation of the references to colour in this figure legend, the reader is referred to the web version of this article.)

The mathematical analysis of these kinetic curves is not conclusive, because there are only 3 experimental points in the useful time range before the completion of the process. Increasing the time resolution of the kinetic experiments is not possible, because the centrifugation time of the samples for the ICP analysis is limiting.

The very fast binding of Pd(II) implies that due to the highly permeable pore structure of the aerogel, the rate-determining step is the direct chemical interaction between the binding sites and the metal ions, which is characteristic for chemisorption [72,73].

An important observation is that at higher initial Pd(II) concentrations, the aqueous Pd(II) concentration slightly decreases in a secondary slow process after 2 h. This is further verified using fresh Pd(II) solutions as reference. The explanation for this secondary process is that the extensive agitation of the solution can result in the formation of the carbonate precipitate of Pd(II) when the system is not deaerated. In order to avoid these complications, the optimum contact time for the sorption process is established to be 2 h.

3.3. Recovery of Pd(II), sorbent regeneration

The dissolution and recovery of Pd(II) was realized by suspending the equilibrated aerogel pellets produced in the batch sorption experiments in solutions of different soft Lewis base ligands capable of forming aqueous complexes with Pd(II) [74,75]. This approach provides information on the reversibility of the binding of Pd(II), as well. Approximately 60% of the bound Pd(II) can be recovered using 5.0 mM cysteine solution in a single washing step. Complete recovery (96–103%) was achieved by washing the equilibrated aerogel pellet with 5.0 mM methionine solution. These results also demonstrate that the binding of Pd(II) is reversible, and the metal ions are not reduced on the surface of the aerogel.

The recycling of the aerogel sorbent was tested by performing consecutive sorption-regeneration cycles. The aerogel retained 94 ± 3% of its sorption capacity after 2 cycles of regeneration by methionine. After 3 sorption-regeneration cycles, the regenerated SG-COOH showed a significant decrease in sorption capacity. This is attributed to the chemical degradation of the aerogel backbone and the surface functional groups in the acidic solutions.

3.4. Mechanism of sorption of Pd(II) on SG-COOH

Several factors have an effect on the kinetic and thermodynamic characteristics of the sorption of Pd(II) on SG-COOH. The most important aspects in terms of the metal ion are its hydrolysis, solubility and the

presence of complexing ligands in the solution phase. In terms of the sorbent, the morphological characteristics (particle size, porosity, pore permeability, etc.), and the chemical properties (number of active sites, availability of donor atoms, protonation state of functional groups, interaction of active sites, possibility for metal ion chelation, etc.) are decisive.

3.4.1. Binding mode of Pd(II) by XPS and FT-IR

The XPS survey spectra of the pristine and the Pd(II) equilibrated SG-COOH together with the high resolution spectrum of Pd 3d of the latter system are shown in Fig. 12. Evidently, the Pd signals are present only in the spectrum of the equilibrated sorbent and missing from that of the pristine one. The assignation of the survey scan peaks and the deconvolution of the Pd 3d spectra are presented in Fig. 12.

The mathematical analysis of the high resolution spectrum revealed that the Pd 3d peaks correspond to a single component that is unambiguously a + 2 oxidation state palladium species [76]. There is no elementary palladium in the system, i.e. the reduction of Pd(II) does not take place even as a side reaction during sorption. This is in good accordance with the 100% recovery of Pd(II) by methionine, as described in Section 3.3. The binding energies of the bound Pd(II) (Pd $3d_{5/2}$: 337.6 eV and Pd $3d_{5/2}$: 342.9 eV) correspond well to those measured in compounds where Pd(II) is in strong coordination by O-atoms of carboxylate groups [76–78]. The Pd 3d binding energies are significantly lower than the present values when Pd(II) is coordinated by N-atoms in amines, or by S-atoms in thiourea moieties [29,79]. Thus, the binding mode of Pd(II) in the equilibrated SG-COOH is reversible complexation by the adjacent carboxylate groups via strong coordinative covalent bonds to O-atoms.

The FT-IR spectrum of the pristine SG-COOH was taken before using it in a sorption experiment, and after equilibrating it with aqueous Pd (II). The same conditions were used as for the XPS study. The equilibrated aerogel pellet of the typical batch experiment was dried under ambient conditions in air at 40 °C for 16 h. It is important to note, that this drying causes the collapse of the porous network of the aerogel, which can be accompanied by other structural changes, as well. Nevertheless, the sorption of Pd(II) caused dramatic and specific changes in some particular FT-IR peaks of the equilibrated aerogel (Fig. 13). Dramatic shifts were observed exclusively at around 1600–1720 cm^{-1} in the peaks assigned to C=O stretching vibrations, and especially in the peak at 1718 cm^{-1} assigned to the free carboxylic groups of the pristine SG-COOH. Thus, the FT-IR provides additional evidence that the large amount of the bound Pd(II) ions are in strong interaction with these O-containing functional groups. Similar changes

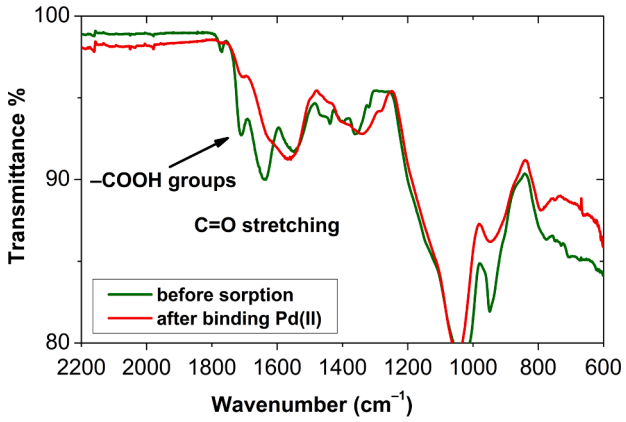

Fig. 13. The FT-IR spectra of the pristine SG-COOH (red) and the that of a dried aerogel pellet equilibrated with aqueous Pd(II) (green), which was recovered from a typical batch sorption experiment. The spectrum of the dried aerogel pellet is somewhat distorted because of the collapse of the pore network due to the ambient drying. The amount of bound Pd(II) was q_E = 166 mg/g in the equilibrated aerogel. (For interpretation of the references to colour in this figure legend, the reader is referred to the web version of this article.)

were observed in the FT-IR peaks of the carboxylate groups of cross-linked alginate aerogels upon the binding of lanthanide ions [80]. The authors explained this by the complex formation between the metal ions and the carboxylic groups.

3.4.2. Surface complexation

Based on the experimental observations, the mechanism of sorption of Pd(II) on SG-COOH aerogel is surface complexation (Scheme 2) [81,82]. This is strongly supported by the fact that Pd(II) selectively binds to SG-COOH and no other cation shows affinity towards the aerogel. Furthermore, the XPS data suggest that the carboxylate groups in close proximity are the primary actives sites binding Pd(II) via coordinative covalent bonds. Adjacent carboxylate groups are known to form very stable complexes with Pd(II) [68,69]. The complexation is strong enough for displacing other flexible ligands (e.g., OH^- and Cl^-) from the coordination sphere of Pd(II) ions, and broken only using a high concentration of soft Lewis base ligands, such as methionine (cf. Section 3.3).

Besides the hydrolysis of the metal ion, the protonation state of the carboxylate groups must be taken into account when describing the mechanism of binding (cf. Section 3.2.3). The latter equilibria can be

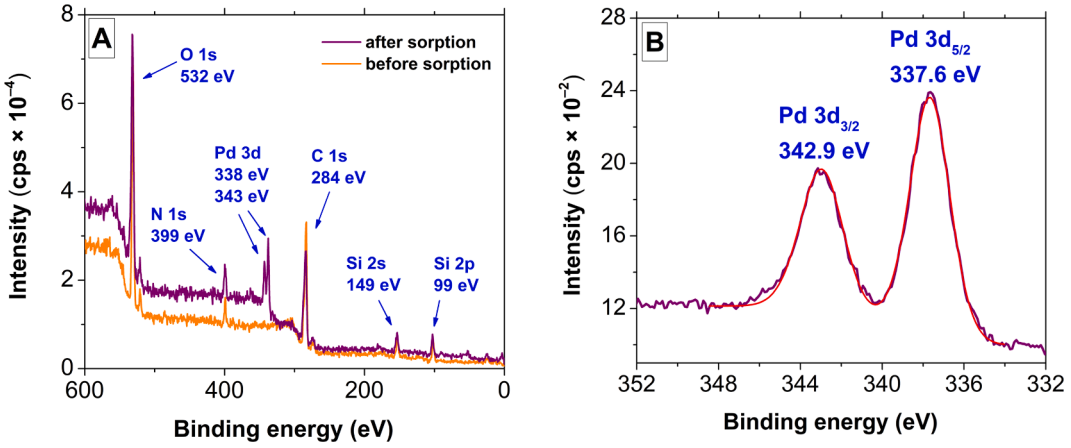

Fig. 12. Panel A: The XPS survey spectra of the pristine SG-COOH (before sorption) and the Pd(II) equilibrated SG-COOH (after sorption). The assignation of the peaks are given in the figure. Panel B: High resolution XPS spectrum of the Pd 3d peaks of the Pd(II) equilibrated SG-COOH (purple line), and the deconvolution of these peaks with a single palladium species (red line) corresponding to +2 oxidation state. The amount of bound Pd(II) was q_E = 166 mg/g in the equilibrated aerogel. (For interpretation of the references to colour in this figure legend, the reader is referred to the web version of this article.)

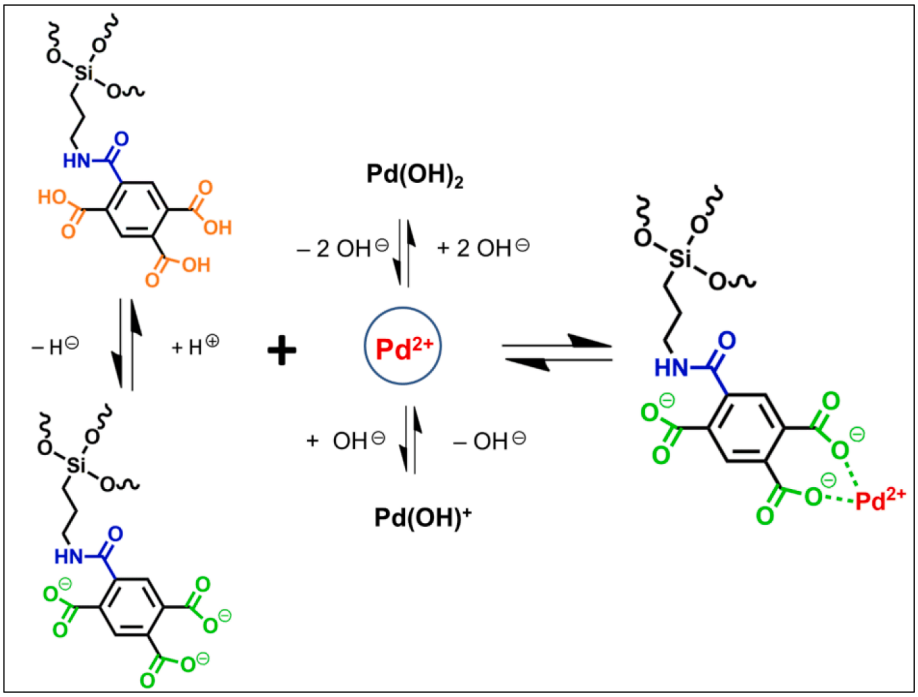

Scheme 2. The proposed mechanism of the binding of Pd(II) to the SG-COOH aerogel and the coupled equilibrium processes.

characterized macroscopically by the isoelectric point of the aerogel, which lies close to pH = 3.0, meaning that at least a portion of the carboxylate groups are protonated in the applied pH range of 2.0–2.3. (For reference, the pK_a values of pyromellitic acid are 1.97; 2.86; 4.46; 6.54.) However, the driving force for the coordination of Pd(II) is strong enough to induce the removal of these protons in favor of the complexation of the metal ions, as described in several cases when Pd(II) coordinates to O-donor ligands [83,84].

Incorporating all of the above considerations, Scheme 2 shows the proposed binding mechanism, which takes into account both the speciation (hydrolysis) of Pd(II) in the aqueous phase, and the protonation state of the functional groups in the aerogel. The strong binding of Pd(II) is expected by the coordination of 2 adjacent carboxylate groups in the equatorial plane, which is a preferential complexation mode of Pd (II) [77,78,85]. Besides this coordination mode, several other minor species are possible, e.g. the monodentate binding of O-donors, or N-donors, such as amino groups in the protein side chains of gelatin. Interactions among functional groups in close proximity are also possible. The presence of multiple binding modes are verified by the complicated nature of the experimental sorption isotherms (cf. Fig. 8), which can adequately be fitted only using the Sips model developed for the description of sorbents with multiple binding modes but limiting monolayer coverage. However, these minor binding modes cannot be detected in the Pd 3d XPS peaks of bound Pd(II), not even by deconvolution.

3.5. Comparison with other sorbents

The SG-COOH aerogel is a high performance and selective Pd(II) sorbent at highly acidic pH, which is a major advantage considering practical applications. The maximum sorption capacity of the SG-COOH aerogel is well above 200 mg g^{-1}, which significantly exceeds the capacities of the previously reported Pd(II) sorbents tested in acidic media. A summary of some recently published Pd(II) sorbents is given in Table 4, and ref. [12] offers a comprehensive review on the topic. When benchmarking the sorbents, it is important to emphasize that sorption capacities reported at pH values higher than 3.0 are burdened with a positive error, because of the spontaneous hydrolysis and precipitation of Pd(II), as discussed in the previous sections of this paper and in the literature [86].

Table 4
Comparison of the performance of some recently published Pd(II) sorbents.

Sorbent	Selectivity	Sorption capacity for Pd (II) (mg g^{-1})	pH	ref.
Polycarboxylate functionalized silica-gelatin aerogel	Pd(II)	369	2.3	this work
Thiourea-modified chitosan microspheres	Pt(IV) and Pd (II)	112	2.0	[10]
Thiourea-modified diethylaminoethyl-cellulose	Pt(IV) and Pd (II)	112	1.1	[18]
Ethylenediamine-modified magnetic chitosan nanoparticles	Pt(IV) and Pd (II)	138	2.0	[19]
Glycine-modified crosslinked chitosan	Au(III), Pt(IV) and Pd(II)	120	2.0	[21]
Crosslinked chitosan/ montmorillonite	N.A.	193	2.0	[22]
Rubeanic acid grafted crosslinked chitosan	N.A.	345	2.0	[86]

Another important advantage of the SG-COOH aerogel is its remarkable selectivity for Pd(II). Most of the sorbents developed for the recovery of Pd(II) also show significant affinities toward platinum ions (cf. Table 4 and ref. [12]), whereas the SG-COOH aerogel enables the separation of these valuable compounds with very similar chemical properties. Furthermore, both the sorption of Pd(II), and its dissolution and recovery by methionine are fast processes, which is beneficial for the functionality of the aerogel sorbent. The quantitative recovery of Pd (II) and the regeneration of the sorbent is possible with a dilute (5 mM) solution of methionine, which is an inexpensive amino acid, and naturally eco-friendly.

4. Conclusions

A supercritically dried polycarboxylate (pyromellitic acid monoamide) functionalized silica-gelatin aerogel was developed for the selective sorption of aqueous Pd(II). The hydrated aerogel has an open and permeable, mainly meso- and macroporous framework with a high specific surface area. The functionalized aerogel shows exceptionally high selectivity for the sorption of aqueous Pd(II), which prevails in competition with Pt(II) and Pt(IV) even at longer contact times and higher temperatures. The optimal pH range for the sorption of Pd(II) is pH = 2.0–2.3 taking into consideration both the hydrolysis of metal ion and the protonation of the carboxylate functional groups in the aerogel. The experimental sorption isotherms can adequately be fitted by the Sips model, which accounts for the existence of multiple dynamic equilibria in different binding modes and the limiting monolayer coverage of the surface. The sorption capacity for Pd(II) is estimated to be 369 mg g^{-1} at pH = 2.3. This sorption capacity is significantly higher than the previously reported values for advanced Pd(II) sorbents. Further practical advantages of the aerogel are that the sorption equilibrium is established in 2 h of contact time, and the quantitative recovery of Pd(II) can be realized using a 5.0 mM methionine solution. The mechanism of Pd(II) binding is the reversible surface complexation of the metal ion by the adjacent carboxylate functional groups, which is a preferential coordination mode of Pd(II) and accounts for the excellent selectivity of the sorbent, as well.

CRediT authorship contribution statement

Petra Herman: Methodology, Validation, Formal analysis, Data curation, Investigation, Writing – original draft, Visualization. **Krisztián Moldován:** Methodology, Validation, Formal analysis, Investigation. **Geo Paul:** Methodology, Validation, Formal analysis, Investigation. **Leonardo Marchese:** Methodology, Validation, Formal analysis. **Zoltán Balogh:** Methodology, Validation, Formal analysis, Investigation. **Adél Len:** Methodology, Validation, Formal analysis. **Zoltán Dudás:** Methodology, Validation, Formal analysis. **István Fábián:** Conceptualization, Resources, Supervision, Funding acquisition. **József Kalmár:** Methodology, Validation, Formal analysis, Data curation, Conceptualization, Validation, Resources, Writing – original draft, Writing – review & editing, Supervision.

Declaration of Competing Interest

The authors declare that they have no known competing financial interests or personal relationships that could have appeared to influence the work reported in this paper.

Data availability

Data will be made available on request.

Acknowledgments

The research has been financially supported by the National Research, Development and Innovation Office, Hungarian Science Foundation (OTKA: FK_17-124571). J.K. is grateful for the János Bolyai Research Scholarship of the Hungarian Academy of Sciences and for the New National Excellence Program (ÚNKP-21-5 Bolyai+) of Ministry of Innovation and Technology of Hungary for financial support.

Appendix A. Supplementary material

Supplementary data to this article can be found online at https://doi.org/10.1016/j.apsusc.2022.156026.

References

[1] C.C. Johansson Seechurn, M.O. Kitching, T.J. Colacot, V. Snieckus, Palladium-catalyzed cross-coupling: a historical contextual perspective to the 2010 Nobel Prize, Angew. Chem. 51 (2012) 5062–5085, https://doi.org/10.1002/anie.201107017.
[2] E.-I. Negishi, Q. Hu, Z. Huang, M. Qian, G. Wang, H. Brown, Palladium-catalyzed alkenylation by the Negishi coupling, Aldrichim. Acta 38 (2005) 71–87, https://doi.org/10.1002/chin.200638271.
[3] J.P. Wolfe, R.A. Singer, B.H. Yang, S.L. Buchwald, Highly active palladium catalysts for suzuki coupling reactions, J. Am. Chem. Soc. 121 (1999) 9550–9561, https://doi.org/10.1021/ja992130h.
[4] Y. Jiang, D. Kim, Synthesis and selective adsorption behavior of Pd(II)-imprinted porous polymer particles, Chem. Eng. J. 232 (2013) 503–509, https://doi.org/10.1016/j.cej.2013.08.008.
[5] F.L. Bernardis, R.A. Grant, D.C. Sherrington, A review of methods of separation of the platinum-group metals through their chloro-complexes, React. Funct. Polym. 65 (2005) 205–217, https://doi.org/10.1016/j.reactfunctpolym.2005.05.011.
[6] M. Hartings, Reactions coupled to palladium, Nat. Chem. 4 (2012) 764, https://doi.org/10.1038/nchem.1437.
[7] R.M. Izatt, S.R. Izatt, N.E. Izatt, K.E. Krakowiak, R.L. Bruening, L. Navarro, Industrial applications of molecular recognition technology to separations of platinum group metals and selective removal of metal impurities from process streams, Green Chem. 17 (2015) 2236–2245, https://doi.org/10.1039/c4gc02188f.
[8] C.E. Garrett, K. Prasad, The art of meeting palladium specifications in active pharmaceutical ingredients produced by Pd-catalyzed reactions, Adv. Synth. Catal. 346 (2004) 889–900, https://doi.org/10.1002/adsc.200404071.
[9] K. Kohler, R.G. Heidenreich, S.S. Soomro, S.S. Prockl, Supported palladium catalysts for suzuki reactions: structure-property relationships, optimized reaction protocol and control of palladium Leaching, Adv. Synth. Catal. 350 (2008) 2930–2936, https://doi.org/10.1002/adsc.200800575.
[10] L. Zhou, J. Liu, Z. Liu, Adsorption of platinum(IV) and palladium(II) from aqueous solution by thiourea-modified chitosan microspheres, J. Hazard. Mater. 172 (2009) 439–446, https://doi.org/10.1016/j.jhazmat.2009.07.030.
[11] A. Abidli, Y. Huang, Z. Ben Rejeb, A. Zaoui, C.B. Park, Sustainable and efficient technologies for removal and recovery of toxic and valuable metals from wastewater: Recent progress, challenges, and future perspectives, Chemosphere 292 (2022), 133102, https://doi.org/10.1016/j.chemosphere.2021.133102.
[12] S. Sharma, A.S.K. Kumar, N. Rajesh, A perspective on diverse adsorbent materials to recover precious palladium and the way forward, RSC Adv. 7 (2017) 52133–52142, https://doi.org/10.1039/C7RA10153H.
[13] H. Narita, K. Morisaku, K. Tamura, M. Tanaka, H. Shiwaku, Y. Okamoto, S. Suzuki, T. Yaita, Extraction properties of palladium(II) in HCl solution with sulfide-containing monoamide compounds, Ind. Eng. Chem. Res. 53 (2014) 3636–3640, https://doi.org/10.1021/ie404363b.
[14] V.T. Nguyen, J.-C. Lee, A. Chagnes, M.-S. Kim, J. Jeong, G. Cote, Highly selective separation of individual platinum group metals (Pd, Pt, Rh) from acidic chloride media using phosphonium-based ionic liquid in aromatic diluent, RSC Adv. 6 (2016) 62717–62728, https://doi.org/10.1039/C6RA09328K.
[15] W. Wei, C.-W. Cho, S. Kim, M.-H. Song, J.K. Bediako, Y.-S. Yun, Selective recovery of Au(III), Pt(IV), and Pd(II) from aqueous solutions by liquid–liquid extraction using ionic liquid Aliquat-336, J. Mol. Liq. 216 (2016) 18–24, https://doi.org/10.1016/j.molliq.2016.01.016.
[16] S. Rajendran, A.K. Priya, P. Senthil Kumar, T.K.A. Hoang, K. Sekar, K.Y. Chong, K. S. Khoo, H.S. Ng, P.L. Show, A critical and recent developments on adsorption technique for removal of heavy metals from wastewater-A review, Chemosphere 303 (2022), 135146, https://doi.org/10.1016/j.chemosphere.2022.135146.
[17] K. Fujiwara, A. Ramesh, T. Maki, H. Hasegawa, K. Ueda, Adsorption of platinum (IV), palladium (II) and gold (III) from aqueous solutions onto l-lysine modified crosslinked chitosan resin, J. Hazard. Mater. 146 (2007) 39–50, https://doi.org/10.1016/j.jhazmat.2006.11.049.
[18] M.H. Morcali, B. Zeytuncu, S. Akman, O. Yucel, Preparation and sorption behavior of DEAE-cellulose-thiourea-glutaraldehyde sorbent for Pt(IV) and Pd(II) from leaching solutions, Desalin. Water Treat. 57 (2016) 6582–6593, https://doi.org/10.1080/19443994.2015.1010591.
[19] L. Zhou, J. Xu, X. Liang, Z. Liu, Adsorption of platinum(IV) and palladium(II) from aqueous solution by magnetic cross-linking chitosan nanoparticles modified with ethylenediamine, J. Hazard. Mater. 182 (2010) 518–524, https://doi.org/10.1016/j.jhazmat.2010.06.062.
[20] M. Ruiz, A.M. Sastre, E. Guibal, Palladium sorption on glutaraldehyde-crosslinked chitosan, React. Funct. Polym. 45 (2000) 155–173, https://doi.org/10.1016/S1381-5148(00)00019-5.
[21] A. Ramesh, H. Hasegawa, W. Sugimoto, T. Maki, K. Ueda, Adsorption of gold(III), platinum(IV) and palladium(II) onto glycine modified crosslinked chitosan resin, Bioresour. Technol. 99 (2008) 3801–3809, https://doi.org/10.1016/j.biortech.2007.07.008.
[22] J. Liu, L. Zheng, Y. Li, M. Free, M. Yang, Adsorptive recovery of palladium(ii) from aqueous solution onto cross-linked chitosan/montmorillonite membrane, RSC Adv. 6 (2016) 51757–51767, https://doi.org/10.1039/C6RA06731J.
[23] S. Sharma, N. Rajesh, Expeditious preparation of β-cyclodextrin grafted chitosan using microwave radiation for the enhanced palladium adsorption from aqueous waste and an industrial catalyst, J. Environ. Chem. Eng. 5 (2017) 1927–1935, https://doi.org/10.1016/j.jece.2017.03.015.

[24] S. Sharma, M. Barathi, N. Rajesh, Efficacy of a heterocyclic ligand anchored biopolymer adsorbent for the sequestration of palladium, Chem. Eng. J. 259 (2015) 457–466, https://doi.org/10.1016/j.cej.2014.08.002.

[25] S. Sharma, N. Rajesh, 2-Mercaptobenzothiazole impregnated cellulose prepared by ultrasonication for the effective adsorption of precious metal palladium, Chem. Eng. J. 241 (2014) 112–121, https://doi.org/10.1016/j.cej.2013.12.002.

[26] F. Bai, G. Ye, G. Chen, J. Wei, J. Wang, J. Chen, Highly selective recovery of palladium by a new silica-based adsorbent functionalized with macrocyclic ligand, Sep. Purif. Technol. 106 (2013) 38–46, https://doi.org/10.1016/j.seppur.2012.12.021.

[27] M.R. Awual, M.A. Khaleque, Y. Ratna, H. Znad, Simultaneous ultra-trace palladium (II) detection and recovery from wastewater using new class meso-adsorbent, J. Ind. Eng. Chem. 21 (2015) 405–413, https://doi.org/10.1016/j.jiec.2014.02.053.

[28] S. Sharma, C.-M. Wu, R.T. Koodali, N. Rajesh, An ionic liquid-mesoporous silica blend as a novel adsorbent for the adsorption and recovery of palladium ions, and its applications in continuous flow study and as an industrial catalyst, RSC Adv. 6 (2016) 26668–26678, https://doi.org/10.1039/C5RA26673D.

[29] R. Nagarjuna, S. Sharma, N. Rajesh, R. Ganesan, Effective adsorption of precious metal palladium over polyethyleneimine-functionalized alumina nanopowder and its reusability as a catalyst for energy and environmental applications, ACS Omega 2 (2017) 4494–4504, https://doi.org/10.1021/acsomega.7b00431.

[30] T. Kang, Y. Park, J. Yi, Highly selective adsorption of Pt2+ and Pd2+ using thiol-functionalized mesoporous silica, Ind. Eng. Chem. Res. 43 (2004) 1478–1484, https://doi.org/10.1021/ie030590k.

[31] L. Liu, S. Liu, Q. Zhang, C. Li, C. Bao, X. Liu, P. Xiao, Adsorption of Au(III), Pd(II), and Pt(IV) from aqueous solution onto graphene oxide, J. Environ. Chem. Eng. 58 (2013) 209–216, https://doi.org/10.1021/je300551c.

[32] S. Sharma, N. Rajesh, Synergistic influence of graphene oxide and tetraoctylammonium bromide (frozen ionic liquid) for the enhanced adsorption and recovery of palladium from an industrial catalyst, J. Chem. Eng. Data 4 (2016) 4287–4298, https://doi.org/10.1016/j.jece.2016.09.028.

[33] L. Liu, C. Li, C. Bao, Q. Jia, P. Xiao, X. Liu, Q. Zhang, Preparation and characterization of chitosan/graphene oxide composites for the adsorption of Au (III) and Pd(II), Talanta 93 (2012) 350–357, https://doi.org/10.1016/j.talanta.2012.02.051.

[34] H. Sharififard, M. Soleimani, F.Z. Ashtiani, Evaluation of activated carbon and bio-polymer modified activated carbon performance for palladium and platinum removal, J. Taiwan Inst. Chem. Eng. 43 (2012) 696–703, https://doi.org/10.1016/j.jtice.2012.04.007.

[35] E. Birinci, M. Gülfen, A.O. Aydın, Separation and recovery of palladium(II) from base metal ions by melamine–formaldehyde–thiourea (MFT) chelating resin, Hydrometallurgy 95 (2009) 15–21, https://doi.org/10.1016/j.hydromet.2008.04.002.

[36] O.E. Fayemi, A.S. Ogunlaja, P.F.M. Kempgens, E. Antunes, N. Torto, T. Nyokong, Z. R. Tshentu, Adsorption and separation of platinum and palladium by polyamine functionalized polystyrene-based beads and nanofibers, Miner. Eng. 53 (2013) 256–265, https://doi.org/10.1016/j.mineng.2013.06.006.

[37] Z. Hubicki, A. Wołowicz, Adsorption of palladium(II) from chloride solutions on Amberlyst A 29 and Amberlyst A 21 resins, Hydrometallurgy 96 (2009) 159–165, https://doi.org/10.1016/j.hydromet.2008.10.002.

[38] R. Ruhela, K.K. Singh, B.S. Tomar, J.N. Sharma, M. Kumar, R.C. Hubli, A.K. Suri, Amberlite XAD-16 functionalized with 2-acetyl pyridine group for the solid phase extraction and recovery of palladium from high level waste solution, Sep. Purif. Technol. 99 (2012) 36–43, https://doi.org/10.1016/j.seppur.2012.08.018.

[39] S. Sharma, N. Rajesh, Augmenting the adsorption of palladium from spent catalyst using a thiazole ligand tethered on an amine functionalized polymeric resin, Chem. Eng. J. 283 (2016) 999–1008, https://doi.org/10.1016/j.cej.2015.08.061.

[40] M. Li, S. Tang, Z. Zhao, X. Meng, F. Gao, S. Jiang, Y. Chen, J. Feng, C. Feng, A novel nanocomposite based silica gel/graphene oxide for the selective separation and recovery of palladium from a spent industrial catalyst, Chem. Eng. J. 386 (2020), 123947, https://doi.org/10.1016/j.cej.2019.123947.

[41] H. Yu, P. Shao, L. Fang, J. Pei, L. Ding, S.G. Pavlostathis, X. Luo, Palladium ion-imprinted polymers with PHEMA polymer brushes: Role of grafting polymerization degree in anti-interference, Chem. Eng. J. 359 (2019) 176–185, https://doi.org/10.1016/j.cej.2018.11.149.

[42] J.P. Vareda, A.J.M. Valente, L. Duraes, Assessment of heavy metal pollution from anthropogenic activities and remediation strategies: a review, J. Environ. Manag. 246 (2019) 101–118, https://doi.org/10.1016/j.jenvman.2019.05.126.

[43] A. James, D. Yadav, Bioaerogels, the emerging technology for wastewater treatment: a comprehensive review on synthesis, properties and applications, Environ. Res. 212 (2022), 113222, https://doi.org/10.1016/j.envres.2022.113222.

[44] E. Georgiou, G. Raptopoulos, M. Papastergiou, P. Paraskevopoulou, I. Pashalidis, Extremely efficient uranium removal from aqueous environments with polyurea-cross-linked alginate aerogel beads, ACS Appl. Polym. Mater. 4 (2022) 920–928, https://doi.org/10.1021/acsapm.1c01400.

[45] P. Herman, A. Kiss, I. Fabian, J. Kalmar, G. Nagy, In situ remediation efficacy of hybrid aerogel adsorbent in model aquatic culture of Paramecium caudatum exposed to Hg(II), Chemosphere 275 (2021), 130019, https://doi.org/10.1016/j.chemosphere.2021.130019.

[46] M. Kéri, A. Forgács, V. Papp, I. Bányai, P. Veres, A. Len, Z. Dudás, I. Fábián, J. Kalmár, Gelatin content governs hydration induced structural changes in silica-gelatin hybrid aerogels - Implications in drug delivery, Acta Biomater. 105 (2020) 131–145, https://doi.org/10.1016/j.actbio.2020.01.016.

[47] I. Lázár, I. Fábián, A Continuous extraction and pumpless supercritical CO_2 drying system for laboratory-scale aerogel production, Gels 2 (2016) 26, https://doi.org/10.3390/gels2040026.

[48] S.S. Park, M.H. Jung, Y.-S. Lee, J.-H. Bae, S.-H. Kim, C.-S. Ha, Functionalised mesoporous silica nanoparticles with excellent cytotoxicity against various cancer cells for pH-responsive and controlled drug delivery, Mater. Des. 184 (2019), 108187, https://doi.org/10.1016/j.matdes.2019.108187.

[49] M. Chanda, G.L. Rempel, Polybenzimidazole resin based new chelating-agents - palladium(Ii) and platinum(Iv) sorption on resin with immobilized dithiooxamide, React. Polym. 12 (1990) 83–94, https://doi.org/10.1016/0923-1137(90)90064-B.

[50] I. Lázár, A. Forgács, A. Horváth, G. Király, G. Nagy, A. Len, Z. Dudás, V. Papp, Z. Balogh, K. Moldován, L. Juhász, C. Cserháti, Z. Szántó, I. Fábián, J. Kalmár, Mechanism of hydration of biocompatible silica-casein aerogels probed by NMR and SANS reveal backbone rigidity, Appl. Surf. Sci. 531 (2020), 147232, https://doi.org/10.1016/j.apsusc.2020.147232.

[51] M. Thommes, K. Kaneko, A.V. Neimark, J.P. Olivier, F. Rodriguez-Reinoso, J. Rouquerol, K.S.W. Sing, Physisorption of gases, with special reference to the evaluation of surface area and pore size distribution (IUPAC Technical Report), Pure Appl. Chem. 87 (2015) 1051–1069, https://doi.org/10.1515/pac-2014-1117.

[52] N. Hüsing, U. Schubert, R. Mezei, P. Fratzl, B. Riegel, W. Kiefer, D. Kohler, W. Mader, Formation and structure of gel networks from Si(OEt)4/(MeO)3Si(CH2)3NR'2 mixtures (NR'2 = NH2 or NHCH2CH2NH2), Chem. Mater. 11 (1999) 451–457, https://doi.org/10.1021/cm980756l.

[53] L. Bois, A. Bonhomme, A. Ribes, B. Pais, G. Raffin, F. Tessier, Functionalized silica for heavy metal ions adsorption, Colloid. Surface. A 221 (2003) 221–230, https://doi.org/10.1016/S0927-7757(03)00138-9.

[54] K. Wörmeyer, M. Alnaief, I. Smirnova, Amino functionalised Silica-Aerogels for CO2-adsorption at low partial pressure, Adsorption 18 (2012) 163–171, https://doi.org/10.1007/s10450-012-9390-6.

[55] Z. Li, S.Y. Zhao, M.M. Koebel, W.J. Malfait, Silica aerogels with tailored chemical functionality, Mater. Design 193 (2020), 108833, https://doi.org/10.1016/j.matdes.2020.108833.

[56] A. Forgács, Z. Balogh, M. Andrási, A. Len, Z. Dudás, N.V. May, P. Herman, L. Juhász, I. Fábián, N. Lihi, J. Kalmár, Mechanistic explanation for differences between catalytic activities of dissolved and aerogel immobilized Cu(II) cyclen, Appl. Surf. Sci. 579 (2022), 152210, https://doi.org/10.1016/j.apsusc.2021.152210.

[57] E.M. Anitas, Small-angle scattering from fractals: differentiating between various types of structures, Symmetry 12 (2020) 65, https://doi.org/10.3390/Sym12010065.

[58] G. Porod, Die Röntgenkleinwinkelstreuung von dichtgepackten kolloiden Systemen, Kolloid-Z. 124 (1951) 83–114, https://doi.org/10.1007/BF01512792.

[59] A. Emmerling, J. Fricke, Small-angle scattering and the structure of aerogels, J. Non-Cryst. Solids 145 (1992) 113–120, https://doi.org/10.1016/S0022-3093(05)80439-9.

[60] G. Paul, C. Bisio, I. Braschi, M. Cossi, G. Gatti, E. Gianotti, L. Marchese, Combined solid-state NMR, FT-IR and computational studies on layered and porous materials, Chem. Soc. Rev. 47 (2018) 5684–5739, https://doi.org/10.1039/c7cs00358g.

[61] P. Herman, I. Fabian, J. Kalmar, Mesoporous silica-gelatin aerogels for the selective adsorption of aqueous Hg(II), ACS Appl. Nano Mater. 3 (2020) 195–206, https://doi.org/10.1021/acsanm.9b01903.

[62] K.Y. Foo, B.H. Hameed, Insights into the modeling of adsorption isotherm systems, Chem. Eng. J. 156 (2010) 2–10, https://doi.org/10.1016/j.cej.2009.09.013.

[63] J. Wang, X. Guo, Adsorption isotherm models: classification, physical meaning, application and solving method, Chemosphere 258 (2020), 127279, https://doi.org/10.1016/j.chemosphere.2020.127279.

[64] R. Sips, On the structure of a catalyst surface, J. Chem. Phys. 16 (1948) 490–495, https://doi.org/10.1063/1.1746922.

[65] G. Zhao, X. Wu, X. Tan, X. Wang, Sorption of heavy metal ions from aqueous solutions: a review, Open Colloid Sci. J. 4 (2010) 19–31, https://doi.org/10.2174/1876530001104010019.

[66] J.M. van Middlesworth, S.A. Wood, The stability of palladium(II) hydroxide and hydroxy–chloride complexes: an experimental solubility study at 25–85°C and 1 bar, Geochim. Cosmochim. Acta 63 (1999) 1751–1765, https://doi.org/10.1016/S0016-7037(99)00058-7.

[67] R. Pilny, P. Lubal, L.I. Elding, Thermodynamics for complex formation between palladium(ii) and oxalate, Dalton Trans. 43 (2014) 12243–12250, https://doi.org/10.1039/c4dt01062k.

[68] H. Rasoulzadeh, A. Sheikhmohammadi, M. Abtahi, B. Roshan, R. Jokar, Eco-friendly rapid removal of palladium from aqueous solutions using alginate-diatomite magnano composite, J. Environ. Chem. Eng. 9 (2021), 105954, https://doi.org/10.1016/J.Jece.2021.105954.

[69] J.J. Gair, B.E. Haines, A.S. Filatov, D.G. Musaev, J.C. Lewis, Mono-N-protected amino acid ligands stabilize dimeric palladium(ii) complexes of importance to C-H functionalization, Chem. Sci. 8 (2017) 5746–5756, https://doi.org/10.1039/c7sc01674c.

[70] J. Tang, Y. Chen, S. Wang, D. Kong, L. Zhang, Highly efficient metal-organic frameworks adsorbent for Pd(II) and Au(III) recovery from solutions: Experiment and mechanism, Environ. Res. 210 (2022), 112870, https://doi.org/10.1016/j.envres.2022.112870.

[71] S. Sarioglan, Recovery of palladium from spent activated carbon-supported palladium catalysts, Platin. Met. Rev. 57 (2013) 289–296, https://doi.org/10.1595/147106713X663988.

[72] M. Monier, D.A. Abdel-Latif, Y.G. Abou El-Reash, Ion-imprinted modified chitosan resin for selective removal of Pd(II) ions, J. Colloid Interface Sci. 469 (2016) 344–354, https://doi.org/10.1016/j.jcis.2016.01.074.

[73] A.B. Nastasović, B.M. Ekmeščić, Z.P. Sandić, D.V. Ranđelović, M. Mozetič, A. Vesel, A.E. Onjia, Mechanism of Cu(II), Cd(II) and Pb(II) ions sorption from aqueous solutions by macroporous poly(glycidyl methacrylate-co-ethylene glycol dimethacrylate), Appl. Surf. Sci. 385 (2016) 605–615, https://doi.org/10.1016/j.apsusc.2016.05.165.
[74] T.P. Pitner, E.W. Wilson, R.B. Martin, Properties of palladium(II) complexes of peptides and histidine in basic solutions, Inorg. Chem. 11 (1972) 738–742, https://doi.org/10.1021/ic50110a015.
[75] Z. Nagy, I. Fabian, I. Sovago, Thermodynamic, kinetic and structural studies on the ternary palladium(II) complexes of thioether ligands, J. Inorg. Biochem. 79 (2000) 129–138, https://doi.org/10.1016/s0162-0134(99)00157-9.
[76] L.J. Pang, R. Li, J.T. Hu, L.J. Zhang, M.X. Zhang, C.G. Yang, G.Z. Wu, Functionalized polyethylene fibers for the selective capture of palladium ions from aqueous solution, Appl. Surf. Sci. 433 (2018) 116–124, https://doi.org/10.1016/j.apsusc.2017.10.041.
[77] S. Hermans, M. Wenkin, M. Devillers, Carboxylate-type palladium(II) complexes as soluble precursors for the preparation of carbon-supported Pd/C catalysts, J. Mol. Catal. a-Chem. 136 (1998) 59–68, https://doi.org/10.1016/S1381-1169(98)00015-6.
[78] Z. Huang, C. Wang, J.L. Zhao, S.X. Wang, Y. Zhou, L.B. Zhang, Adsorption behavior of Pd(II) ions from aqueous solution onto pyromellitic acid modified-UiO-66-NH2, Arab. J. Chem. 13 (2020) 7007–7019, https://doi.org/10.1016/j.arabjc.2020.07.007.
[79] H. Alamgholiloo, S. Rostamnia, N. Noroozi Pesyan, Extended architectures constructed of thiourea-modified SBA-15 nanoreactor: A versatile new support for the fabrication of palladium pre-catalyst, Appl. Organomet. Chem. 34 (2020), e5452, https://doi.org/10.1002/aoc.5452.
[80] E. Georgiou, I. Pashalidis, G. Raptopoulos, P. Paraskevopoulou, Efficient removal of polyvalent metal ions (Eu(III) and Th(IV)) from aqueous solutions by polyurea-crosslinked alginate aerogels, Gels 8 (2022) 478, https://doi.org/10.3390/gels8080478.
[81] J.E. Mangold, C.M. Park, H.M. Liljestrand, L.E. Katz, Surface complexation modeling of Hg(II) adsorption at the goethite/water interface using the charge distribution multi-site complexation (CD-MUSIC) model, J. Colloid Interface Sci. 418 (2014) 147–161, https://doi.org/10.1016/j.jcis.2013.10.066.
[82] C. Manfredi, R. Mozzillo, S. Volino, M. Trifuoggi, A. Giarra, V. Gargiulo, M. Alfe, On the modeling of heavy metals and rare earth elements adsorption on colloidal carbon-based nanoparticles, Appl. Surf. Sci. 505 (2020), 144264, https://doi.org/10.1016/j.apsusc.2019.144264.
[83] A. Ozsvath, R. Dioszegi, A.C. Benyei, P. Buglyo, Pd(ii)-Complexes of a novel pyridinone based tripeptide conjugate: solution and solid state studies, Dalton Trans. 49 (2020) 9254–9267, https://doi.org/10.1039/d0dt01396j.
[84] J. Zakrzewska, P. Uznanski, Synthesis and characterization of bis(amine)palladium (II) carboxylate complexes as precursors of palladium nanoparticles, Dalton Trans. 50 (2021) 6933–6948, https://doi.org/10.1039/d1dt00638j.
[85] S.Y. Wang, T. Vincent, J.C. Roux, C. Faur, E. Guibal, Pd(II) and Pt(IV) sorption using alginate and algal-based beads, Chem. Eng. J. 313 (2017) 567–579, https://doi.org/10.1016/j.cej.2016.12.039.
[86] E. Guibal, N.V. Sweeney, T. Vincent, J.M. Tobin, Sulfur derivatives of chitosan for palladium sorption, React. Funct. Polym. 50 (2002) 149–163, https://doi.org/10.1016/S1381-5148(01)00110-9.